Hysteretic Behavior and Strength Capacity of Shallow Embedded Steel Column Bases

Yao Cui[1], Ryota Yamamoto[2], Tomomi Uemura[1], Takuya Nagae[3], Toko Hitaka[4], Masayoshi Nakashima[5]

[1] *Graduate Student, Dept. of Architecture and Architectural Engineering, Kyoto University, Kyoto, Japan*
[2] *M. Eng., Kajima Corporation, Tokyo, Japan*
[3] *Research Fellow, National Research Institute for Earth Science and Disaster Prevention, Miki, Hyogo, Japan*
[4] *Associated Professor, Disaster Prevention Research Institute, Kyoto University, Kyoto, Japan*
[5] *Professor, Disaster Prevention Research Institute, Kyoto University, Kyoto, Japan*
Email: snoopy.cy@steel.mbox.media.kyoto-u.ac.jp

ABSTRACT :

A shallow embedded steel column base consisting of an exposed column base and a covering reinforced concrete (RC) floor slab is examined. A series of tests are conducted for shallow embedded steel column bases subjected to horizontal cyclic loading leading to very large deformations, and the effects of the floor slab on the strength and ductility are examined. By the adjustment of the floor slab thickness and shape, the elastic stiffness, maximum strength and dissipated energy of the shallow embedded column bases increases to 1.1 to 1.5, 1.4 to 2.0, and 1.1 to 2.1 times. Punching shear failure in the floor slab around the column is notable due to the uplift of the base plate. At the end of loading, the punched-out part is completely separated from the rest. Based on the plastic theory, a mechanical model that considers the contributions of the anchor bolts and the bearing and punching shear of the floor slab is proposed to evaluate the maximum strength. The evaluated results have good agreement with the test results, with errors not exceeding 20%.

KEYWORDS: Shallow Embedded Column Base, RC Floor Slab, Cyclic Loading, Punching Shear

1. INTRODUCTION

The exposed column base had been popular for low- to medium-rise structures because of better constructability and low cost, although the embedded column base has greater fixity against rotation than does the exposed column base. In addition, the exposed column base exhibits pinching due to the elongation of anchor bolts in the cyclic loading condition that has to be considered in seismic design. Such pinching hysteretic behavior lowers the energy dissipation. On the other hand, in many cases in actual practice a floor slab covers the exposed column base. The contribution of such a slab to the resistance of the column base is ignored in the current design provisions.

Here, we call such a column base the “shallow embedded column base.” This paper presents a series of tests of the shallow embedded column bases in cyclic loading condition and examines the important design parameters, i.e., the elastic stiffness, maximum strength, energy dissipation of the column base. The effects of the slab thickness, slab configuration, and reinforcement on these properties are also investigated. Additionally, a simple but workable procedure to estimate the maximum strength of the shallow embedded column base is proposed.

2. TEST PROGRAM

2.1. Specimens

The test specimens were designed to investigate the interior column base connections that commonly exist in steel structures in Japan. Eight specimens were fabricated at approximately 2/3 scale, with all specimens having the global dimensions shown in Fig.1. A relatively strong column was used to ensure that the base plate connection and/or the covering slab would initiate the development of damage during cyclic loading before significant deformation or damage developed in the column. All eight specimens comprised a cold-formed, square-tube cross section column (200 mm in the width, with a thickness of 9 or 12 mm), a shop-welded, hot-rolled, square base plate (300 mm and 25 mm in the width and thickness), twelve machined anchor bolts, and a reinforced concrete (RC) foundation beam. Here, the base plate level is the same for all specimens. A RC floor slab ("floor slab" hereinafter) is placed on top of the foundation beam to form a shallow embedded column base.

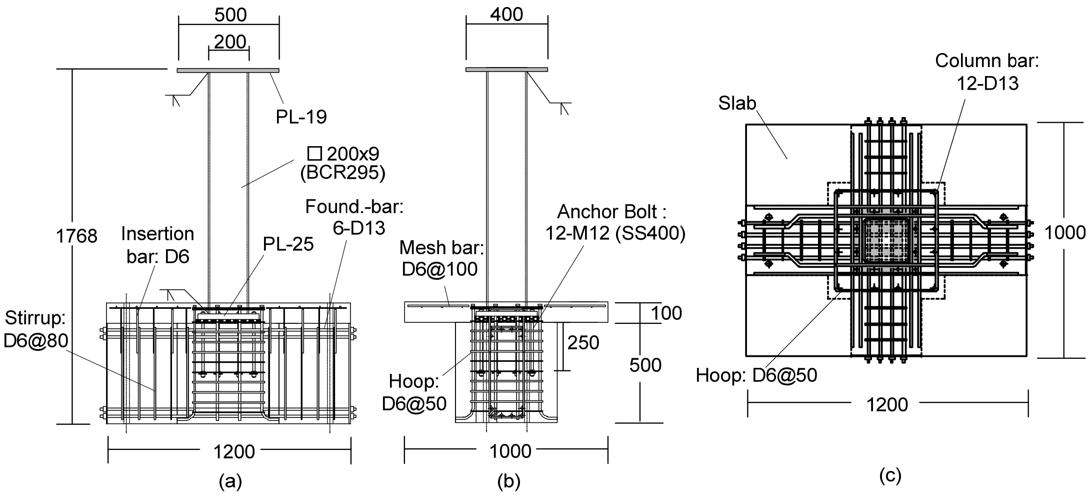

Fig. 1 Test specimen (SL-100-st): (a) front elevation; (b) side elevation; and (c) plane view (unit: mm)

To investigate the floor slab effect on the column base connection, Specimen 'Standard', an exposed column base designed following the associated provisions of Recommendation for Design of Connections in Steel Structures (AIJ, 2006) was fabricated as a baseline specimen. To ensure the anchor bolt fracture, the foundation beam was designed strong enough so that a cone-like failure of concrete would not occur. Normal strength concrete was used for the foundation beam, and high-strength non-shrinkage mortar was adopted to fill in the gap between the base plate and foundation beam.

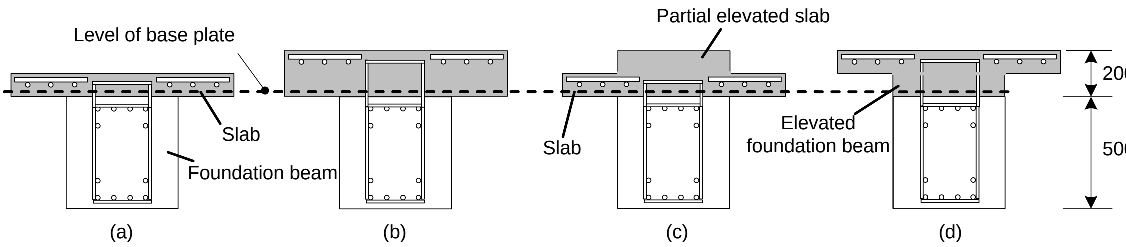

Fig.2 Shape of concrete slab: (a) flat slab type 'SL-100'; (b) flat slab type 'SL-200';
(c) partial elevated slab type 'Foot-100'; and (d) elevated foundation type 'Found.-100'

To investigate the influence of the slab thickness and shape, four specimens (SL-100, SL-200, Foot-100, Found.-100) were designed as shown in Fig. 2. To investigate the influence of rebars, three specimens (SL-100-st, Found.-100-st-t9, and Found.-100-st-t12) with a floor slab strengthened further by eight bent rebars were designed. Deformed reinforcing bars are placed to restrict both the rotation of the base plate and the separation of the floor slab. As shown in Fig. 3, the bent part of the rebars is set approximately perpendicular to the failure surface in the floor slab. All rebars are set around the column and upon the base plate, two pieces at each column side and in each direction. As explained later, Specimen 'Found.-100-st-t9' failed in the column buckling mode because the maximum strength of the base plate connection remained greater than the full plastic moment of the column. To examine the ultimate behavior of this column base configuration, Specimen

'Found.-100-st-t12' with a thicker (12mm) column was prepared as the counterpart of Specimen 'Found.-100-st-t9'.

The material properties of the steel and concrete used for the specimens were obtained from the associated material tests and are summarized in Table 1.

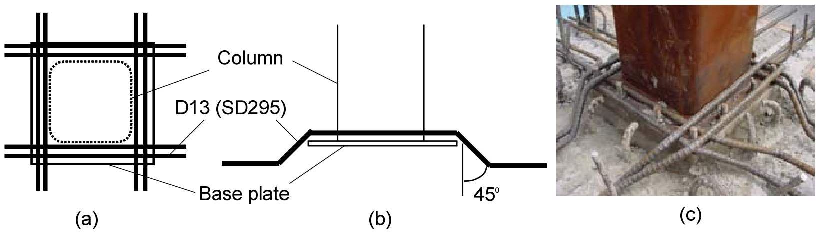

Fig. 3 Configuration of reinforcing bars: (a) plan view; (b) elevation; and (c) arrangement of reinforcing bars

Table 1 Material properties (concrete and steel)

Smapled plates	Steel	Yield strength σ_y (N/mm^2)	Tensile strength σ_u (N/mm^2)
Column	□-200×9, BCR295	387	460
	□-200×12, BCR295	373	412
Column Base	Anchor bolt	306	439
	Base plate	409	546
Slab	Steel bar D13	374	515
	Concrete	30.5	

2.2. Test Setup

The test specimen was placed in the loading frame shown in Fig. 4. The foundation beam was clamped to the reaction floor. The column top was clamped to two oil jacks, one in the horizontal direction and the other in the vertical direction. The specimen was subjected to a constant vertical force of 511 kN, which corresponded to 0.2 times the yield axial load of the column (9 mm thick). A displacement-controlled cyclic load was applied quasi-statically in the horizontal direction. Two cycles were performed at each drift angle, defined as the horizontal displacement at the loading point relative to the height of the column (1238mm). Drift angles of 0.005, 0.015, 0.0225, 0.03, 0.04, 0.06, 0.08, and 0.1 rad were adopted. The test was terminated when the drift angle reached 0.1 rad, or when ten of the twelve anchor bolts fractured, which was regarded as a complete failure.

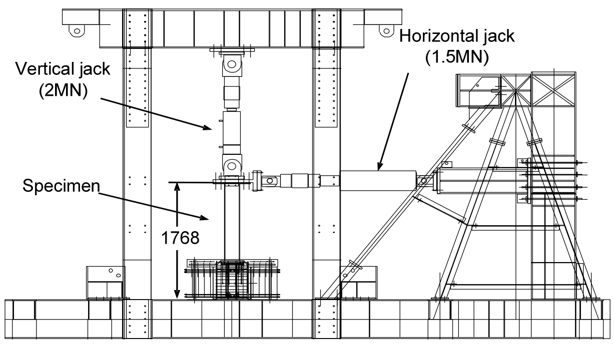

Fig. 4 Elevation of the loading system (unit: mm)

3. TEST RESULT

3.1. Moment-Rotation Relationships

Figure 5 shows the force-deformation relationships for all eight specimens in terms of the end-moment (M)

versus drift angle (θ). The dashed line represents the elastic stiffness of the specimen, which is defined as the secant stiffness between the origin and the point at 0.005 rad. To highlight notable differences in behavior during different deformation ranges, Fig.5 uses two different scales for the abscissa: one scaled to 0.03 rad and the other to 0.12 rad. The drift angle of 0.03 rad was chosen as the maximum rotation that first-story columns, including the column bases of steel moment-resisting frames, may experience in contemporary seismic design. Behavior with rotations greater than 0.03 rad was examined for the seismic capacity of the column base to failure.

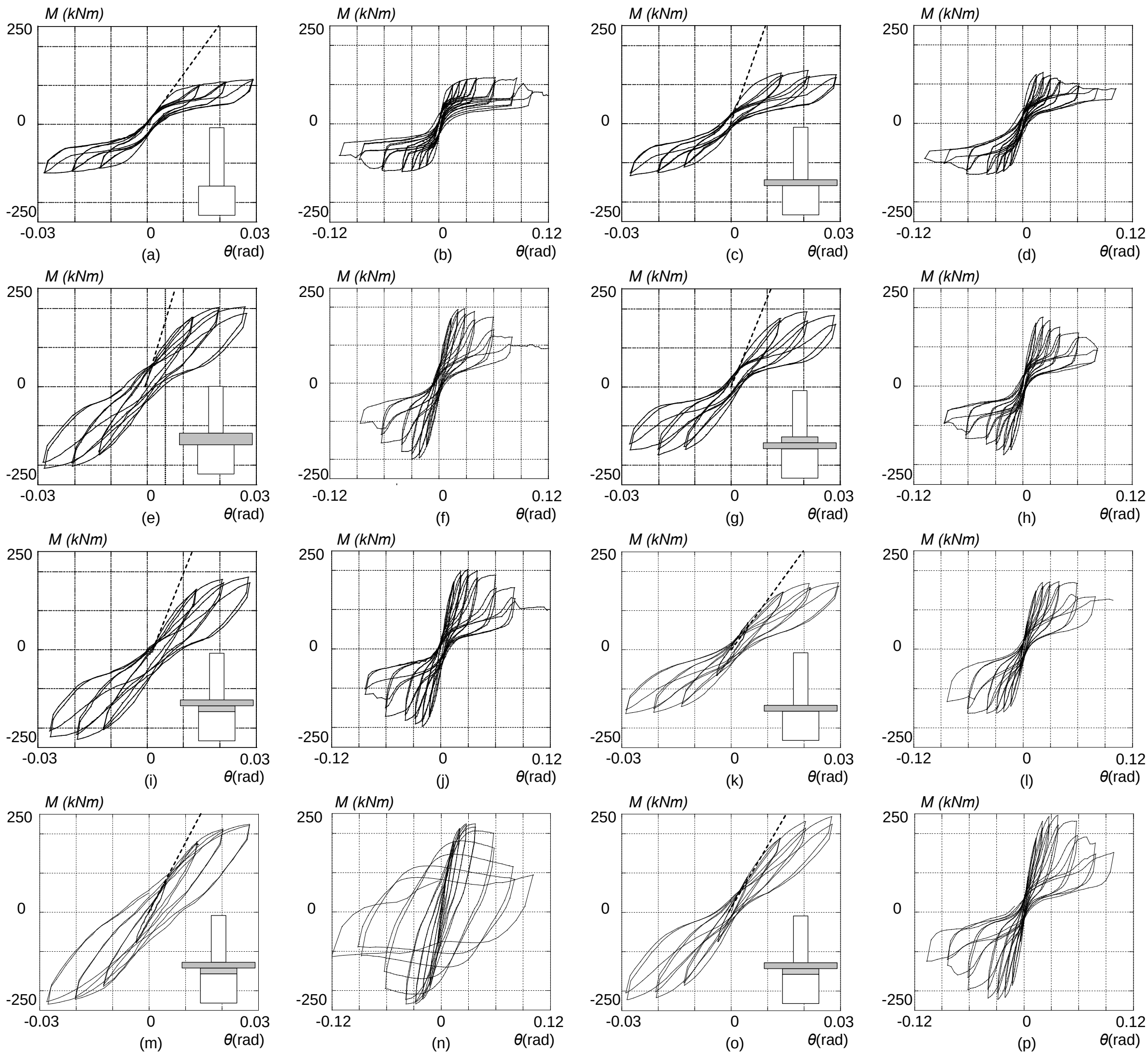

Fig. 5 Moment-rotation relationships: (a) Standard to 0.03 rad; (b) Standard to 0.1 rad; (c) SL-100 to 0.03 rad; (d) SL-100 to 0.1 rad; (e) SL-200 to 0.03 rad; (f) SL-200 to 0.1 rad; (g) Foot-100 to 0.03 rad; (h) Foot-100 to 0.1 rad; (i) Found.-100 to 0.03 rad; (j) Found.-100 to 0.1 rad; (k) SL-100-st to 0.03 rad; (l) SL-100-st to 0.1 rad; (m) Found.-100-st-t9 to 0.03 rad; (n) Found.-100-st-t9 to 0.1 rad; (o) Found.-100-st-t12 to 0.03 rad; and (p) Found.-100-st-t12 to 0.1 rad

In view of the moment-rotation relationships up to the rotation of 0.03 rad, the following observations are notable. Specimen 'Standard' has the smallest maximum strength among all specimens, and the hysteretic loop is severely pinched primarily due to the plastic elongation of the anchor bolts. Other specimens 'SL-200', 'Foot-100', 'Found.-100', 'Found.-100-st-t9', and 'Found.-100-st-t12', show larger maximum strengths and hysteresis loops. The hysteresis loops of specimens with the strengthened slab, i.e., Specimen 'SL-100-st', 'Found.-100-st-t9', and 'Found.-100-st-t12', swell more than those of the corresponding specimens with the floor slab.

In the moment-rotation relationships up to the rotation of 0.1 rad, the specimens exhibited slip behavior similar to that observed in Specimen 'Standard', except for Specimen 'Found.-100-st-t9', the one having the largest hysteresis loops. All specimens arrived at the maximum strength at around 0.03 rad. The strength of the specimens with the floor slab decreased sharply after the maximum strength. The deterioration is due primarily to the punching shear failure of the floor slab, and eventually the strength was lowered to the level of Specimen 'Standard'. On the other hand, specimens with the strengthened slab ('SL-100-st' and 'Found.-100-st-t12') sustained 90% of the maximum strength till the rotation of 0.06 rad. The strength deterioration of these specimens was reduced significantly by the presence of the rebars.

3.2. Failure Mechanism

Two types of failure mode, a column-buckling failure observed in Specimen 'Found.-100-st-t9', as shown in Fig. 6(b), and a punching-shear failure observed in all other specimens, as shown in Fig.6 (a) and (c), occurred in the shallow embedded column base specimens. The failure mode of all specimens that failed in punching shear ('SL-100', 'SL-100-st', 'SL-200', 'Foot-100', 'Found.-100', and 'Found.-100-st-t12') was very similar regardless of the slab shape and reinforcement. The floor slab was uplifted by the rotation of the base plate, and the punching shear failure occurred on the uplifted side. All cracks were connected and formed a cone-like crack during the cycles of 0.03 rad, when the specimen reached the maximum strength. As the column rotation increased, part of the floor slab around the base plate was forced apart. This separation caused the strength deterioration. At the end of loading, a cone with a failure surface radiating from the top of base plate to the surface of the floor slab in a slope angle of about 45° was observed in these specimens.

(a) (b) (c)

Fig. 6 Failure of reinforced specimens: (a) SL-100-st; (b) Found.-100-st-t9; and (c) Found.-100-st-t12

4. EVALUATION OF MAXIMUM RESISTING MOMENT

The level to evaluate the maximum resisting moment is suggested by what happened at the bottom of the base plate. In consideration of the punching shear failure, the model consists of three parts, as shown in Fig. 7，8 and 9, i.e., 1) the exposed column base component, 2) the covering concrete slab component, and 3) the reinforcing bars component. Applying the plastic theory, the strengths of the three parts are added to estimate the maximum moment capacity of the shallow embedded column base.

4.1. Contribution of Exposed Column Bases

The moment capacity of the exposed column base component is estimated by a moment couple that consists of the tension force in the anchor bolts and the equivalent compressive force applied at the centroid of the bearing area under the base plate. M_e is estimated following the procedure adopted in the standard design specifications in Japan (AIJ 2006).

4.2. Contribution of Concrete Slab

The moment resistance of the covering concrete is assumed to be provided by the following two mechanisms: 1) the direct bearing of the slab adjacent to the column in compression (Fig. 7); and 2) the punching resistance in the slab uplifted by the rotation of the base plate (Fig. 8). The relationship between the compressive stress and strain of the concrete is considered to be rigid perfectly-plastic. To employ the assumption of rigid-plasticity, the compressive strength of concrete f_c' is adjusted using two independent effectiveness factors, υ_c and υ_t, for the bearing and punching shear resistance, respectively.

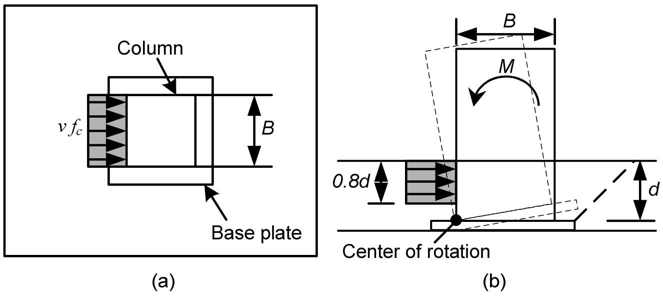

Fig. 7 Model of compressive mechanism in concrete slab: (a) plan view; (b) elevation view

The bearing force is applied at the centroid of the bearing area in the column front surface. It is assumed that concrete yields uniformly in the bearing area. In accordance with the stress block recommended in ACI 318-08 (2008) and AIJ (2006), an effectiveness factor υ_c of 0.85 and an effective depth of 0.8d are adopted. Then, the moment resistance M_{cc} supplied by the concrete in compression is obtained by Eq. (1), with the associated notation defined in Fig.7.

$$M_{cc} = \upsilon_c \cdot f_c' \cdot B \cdot 0.8d \cdot (0.6d + t_{bp}) \tag{1}$$

Where, t_{bp} is the thickness of the base plate.

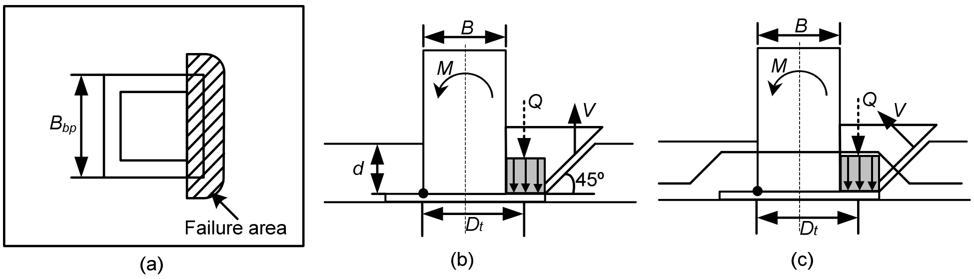

Fig. 8 Model of punching shear mechanism in concrete slab: (a) plan view;
(b) evaluation model for plain concrete slab; and (c) evaluation model for reinforced concrete slab

In reference to the test results, the projected area shown in Fig. 8 (a) is assumed to contribute to the punching resistance. The slope angle of the punching-shear failure surface is assumed to be 45º. The punching-failure mechanism is taken to be the separation of the punched-out concrete with an upward velocity V, while the surrounding slab remains rigid. As shown in Fig. 8 (b) and (c), the direction of the velocity of the punched-out concrete varies with the rebar detail. For the floor slab, it is simply vertical upward. For the strengthened floor slab, since the horizontal rebars were set to prevent the separation caused by the punching failure, the direction of the velocity is taken to be perpendicular upward to the punching-shear surface. The work equation for the assumed failure mechanism is:
For floor slab:

$$Q \cdot V = \frac{1-\sin\alpha}{2} \cdot A \cdot \upsilon_t f_c' \cdot V \tag{2-1}$$

For strengthened floor slab:

$$Q \cdot V \cdot \cos\frac{\pi}{4} = \frac{1-\sin\alpha}{2} \cdot A \cdot \upsilon_t f_c' \cdot V \quad (2\text{-}2)$$

Where Q is the ultimate punching load caused by the base plate, as shown in Fig. 8(b), (c), and A is the area of the punching-shear surface.
Assuming that the punching load caused by the base plate is distributed uniformly, the moment resistance provided by the punching-shear mechanism is evaluated as:

$$M_{ct} = Q \cdot D_t \quad (3)$$

where D_t is the distance between the rotation center of the column base and the centroid of the punching load (250 mm).

4.3. Contribution of Rebars

According to the strain data, it is assumed that a total of eight bent parts of the six rebars located in the punching shear part provide resistance to the rotation of the column base, as shown in Fig. 9. The vertical component of the axial force in the reinforcing bars corresponds to the force that constrains the base plate. Thus, the contribution provided by the reinforcing bars M_{st} is evaluated as follows:

$$M_{st} = T_y \cdot \cos 45° \cdot l \cdot 8 = A_r \sigma_y \cdot \cos 45° \cdot l \cdot 8 \quad (4)$$

Where l is the horizontal distance from the rotation center to reinforcing bars (250 mm); A_r is the cross-sectional area of reinforcing bars (119 mm^2); and σ_y is the yield strength of the reinforcing bars (373 N/mm^2).

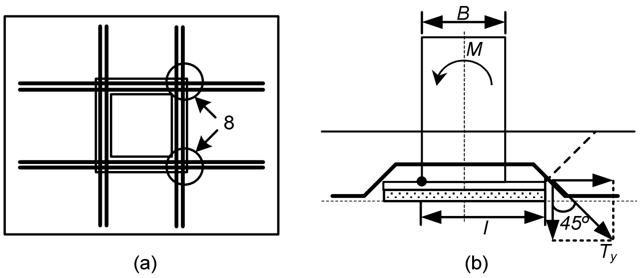

Fig. 9 Model of contribution of reinforcement: (a) plan view; (b) elevation view

4.3. Verification

The contribution to the maximum strength from the floor slab and rebars is taken to be the summation of Eqs. (1), (3), and (4).These calculated ultimate strengths are compared with the corresponding experimental results (shown by black bars) in Fig. 10. For each specimen, the contributions of respective mechanisms are shown separately. The proposed equations generally provide conservative estimates of the moment capacity, with most of the predicted values ranging between 80% and 98% of the corresponding experimental strengths. The ratio of M_{cc} (contribution of the bearing resistance of the floor slab) to M_{ct} (contribution of the punching resistance of the floor slab) changes according to the thickness and shape of the slab. For the specimens with the flat floor slab ('SL-100' and 'SL-200'), the ratio of M_{cc} to M_{ct} increases with the increase of the slab thickness since the slab thickness contributes more to the bearing resistance than does the punching resistance. This is because the bearing and punching resistances are proportional to the square and linear of the slab thickness, respectively. For specimens with partially elevated slabs ('Foot-100'), M_{ct} is relatively small because the failure surface area generated by the punching shear does not increase by the partially elevated portion. For specimens embedded in the foundation beam whose height was increased by an additional 100 mm floor slab ('Found.-100'), the estimated strength is the same as that of the specimen with a floor slab of 200 mm ('SL-200'), because the failure surface area is the same.

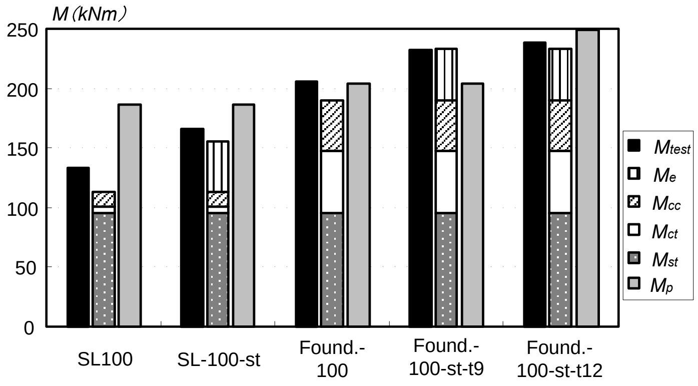

Fig.10 Ultimate strength of specimen

5. CONCLUSIONS

1. The elastic stiffness, maximum strength, and dissipated energy were improved by the presence of the floor slab. The elastic stiffness of the shallow embedded column base specimens was about 1.1 times and 1.5 times for the 100 mm and 200 mm thick floor slabs, respectively. Neither the slab shape nor the horizontal rebars contributed to the elastic stiffness. The configuration (thickness and shape) of the floor slab influenced the maximum strength significantly. The presence of the horizontal rebars further increased the maximum strength. Compared with the baseline exposed column base specimen, the maximum increase was around 1.95 times for the specimen with both the thickest slab and horizontal rebars.
2. The punching shear failure in the floor slab was the main failure mode of the shallow embedded column base. However, the failure mode was converted to the column local buckling mode when the strength of the column base became larger than the full-plastic moment of the column.
3. By using the plastic theory applied to the punching shear failure of the uplifted side of the floor slab and the compressive failure in the compressive side of the floor slab, the maximum strength can be estimated with reasonable accuracy regardless of the thickness and geometric condition of the floor slab. The evaluated results show no more than 20% errors compared with the corresponding test results.

REFERENCES

American Concrete Institute (ACI) (2008). Building Code Requirements for Structural Concrete and Commentary, (ACI 318-08 and 318R-08), ACI, Farmington Hill, Michigan, U.S.A.

Architectural Institute of Japan (AIJ). (1990). Design Guidelines for Earthquake Resistant Reinforced Concrete Buildings Based on Ultimate Strength Concept, Tokyo, Japan. (in Japanese).

Architectural Institute of Japan (AIJ). (2005). Design Standard for Steel Structures- Based on Allowable Stress Concept, Tokyo, Japan. (in Japanese).

Architectural Institute of Japan (AIJ). (2006). Recommendations for Design of Connections in Steel Structures, Tokyo (in Japanese), Japan.

Nielsen, M.P. (1984). Limit Analysis and Concrete Plasticity, Prentice-Hall, Inc., Englewood Cliffs, New Jersey

Richard, M. D. and Sharon, J. E. (1999). Beam-Column Base Plate Design – LRFD Method, *Engineering Journal*, **1st quarter**, 29-38.

Nakashima, S. and Igarashi, S. (1987). Behavior of Steel Square Tubular Column Bases for Interior Columns Embedded in Concrete Footing Under Bending Moment and Shearing Force, Part 2 Initial Stiffness, Ultimate Strength and Mechanism of Stress Flow, *Journal of Structural and Construction Engineering (Transaction of AIJ)*, **374**, 63-76.(in Japanese).